Aharonov-Bohm physics with spin. II. Spin-flip effects in two-dimensional ballistic systems

Diego Frustaglia*
Institut für Theoretische Festkörperphysik, Universität Karlsruhe, 76128 Karlsruhe, Germany

Martina Hentschel
Department of Physics, Duke University, Box 90305, Durham, North Carolina 27708-0305, USA

Klaus Richter
Institut für Theoretische Physik, Universität Regensburg, 93040 Regensburg, Germany
(Received 8 May 2003; revised manuscript received 9 February 2004; published 27 April 2004)

We study spin effects in the magnetoconductance of ballistic mesoscopic systems subject to inhomogeneous magnetic fields. We present a numerical approach to the spin-dependent Landauer conductance which generalizes recursive Green-function techniques to the case with spin. Based on this method we address spin-flip effects in quantum transport of spin-polarized and spin-unpolarized electrons through quantum wires and various two-dimensional Aharonov-Bohm geometries. In particular, we investigate the range of validity of a spin-switch mechanism recently found which allows for controlling spins indirectly via Aharonov-Bohm fluxes. Our numerical results are compared to a transfer-matrix model for one-dimensional ring structures presented in the first paper [Hentschel *et al.*, Phys. Rev. B, preceding paper, Phys. Rev. B **69**, 155326 (2004)] of this series.

DOI: 10.1103/PhysRevB.69.155326 PACS number(s): 73.23.−b, 03.65.Vf, 72.10.−d, 72.25.−b

I. INTRODUCTION

Topological quantum phases, like the Aharonov-Bohm (AB) phase[2] related to interference effects in the presence of a magnetic flux, remain as a source of motivation for the field of mesoscopic physics. Another resource is the spin degree of freedom that is responsible for a rich set of electronic transport phenomena. Examples are manifold and range from applications in the fast growing spintronics sector[3–8] to proposals for quantum information technology.[9–11] Experimental progress in the exploration of these phenomena relies on the fabrication of very clean semiconductor heterostructures, the ability to superimpose complex magnetic structures, and the development of robust spin-injection mechanisms.[12]

In mesoscopic quantum transport, novel spin-related phenomena arise if the spin is coupled to nonuniform magnetic fields. This holds true also for Rashba (spin orbit) effects,[13] which can be regarded as arising from spin coupling to an intrinsic effective magnetic field. In this context, we expect signatures from Berry[14] or geometric phases,[15] topological quantum phases related to the change of the spin orientation upon transport, to become accessible. Recently a number of experiments have been designed for directly manipulating the spin dynamics via externally applied nonuniform magnetic fields with amplitude or direction varying on mesoscopic length scales.[16–19] In this respect, a ring geometry subject to such a textured magnetic field is of particular interest since it represents a favorite setup, at least in principle, for a direct observation of Berry phases[14] in the magnetoconductance.[20,21] The occurence of Berry phases, however, requires adiabatic spin transport and therefore sufficiently strong inhomogenous magnetic fields. Here we will not address the recent discussion[22,23] concerning the necessary conditions to be fulfilled for a clear-cut measurement of such a geometrical phase.

Instead, we study spin-dependent charge transport through ring-type conductors in the entire range from weak to strong spin-magnetic field coupling, i.e., from diabatic to adiabatic spin dynamics. We will show that the interplay between the spatial and spin parts of the involved wave functions leads to subtle interference effects which alter and enrich the usual AB picture of spinless particles.

After introducing our numerical approach to spin-dependent transport in the Landauer framework in Sec. II, we first illustrate in Sec. III basic spin features in the conductance for a simple strip geometry in a nonuniform field. In Sec. IV we investigate two-terminal transport of unpolarized electrons through mesoscopic rings. In Sec. V we then examine in detail and generalize a recently proposed spin-switch mechanism in AB rings.[24] We demonstrate for a large class of two-dimensional systems that this effect can be applied for controlling indirectly (via an AB flux) the spin direction of spin-polarized particles passing through mesoscopic ring geometries.

This is the second paper of a two-paper series on spin-dependent Aharonov-Bohm physics. In the first paper,[1] referred to as paper I in the following, we gave an analytical proof of the spin switch effect for one-dimensional rings. Here we compare our different numerical results with analytical expressions derived in paper I.

II. NUMERICAL APPROACH

In this section we introduce the necessary concepts for studying spin-dependent quantum transport in two-dimensional (2D) mesoscopic systems and outline our method used for the numerical calculation of the magnetoconductance. The conductance of mesoscopic structures is commonly computed using the Landauer formula[25,26] for phase coherent transport in the linear regime (small bias voltage). For leads of width w supporting N open channels (N

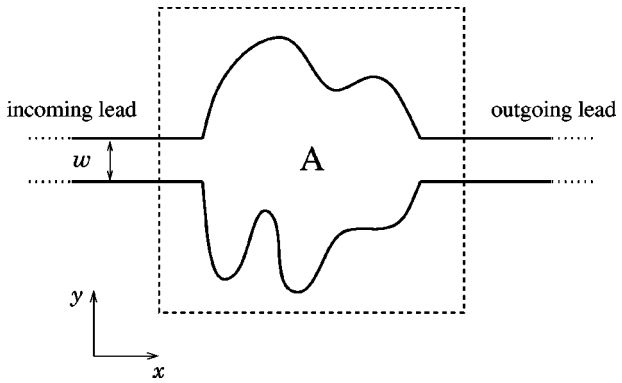

FIG. 1. Two-dimensional conductor of arbitrary shape coupled to two semi-infinite leads of width w defining transverse modes (or channels, with spin s and spatial mode m) in the y direction due to confinement. Particles in channel (s,m) entering the region A from the left are transmitted (reflected) to the right (left) after scattering into channel (s',n).

$=\mathrm{Int}[k_F w/\pi]$) the spin-dependent two-terminal conductance at zero temperature reads

$$G=\frac{e^2}{h}\sum_{n,m=1}^{N}\sum_{s',s}T_{nm}^{s's}. \tag{1}$$

Here, $T_{nm}^{s's}=|t_{nm}^{s's}|^2$ denotes the transmission probability between incoming (m) and outgoing (n) channels with s and s' labeling the spin orientation ($s,s'=\pm 1$ denote spin-up and spin-down states with respect to a certain direction in space). The transmission amplitude $t_{nm}^{s's}$ is obtained by projecting the corresponding spin-dependent Green function $\mathcal{G}$ onto an appropriate set of asymptotic states (spinors) $\{\Phi\}$ defining incoming and outgoing channels.[27] For a 2D microstructure with two attached leads as shown in Fig. 1, the spin-dependent amplitudes read[27,28]

$$t_{nm}^{s's}=-i\hbar(v_n v_m)^{1/2}\int dy'\int dy\,\Phi_n^{s'}{}^*(y')\times\mathcal{G}(x_2,y';x_1,y;E)\Phi_m^s(y). \tag{2}$$

The above equation yields the transmission amplitude of an electron with energy E entering the cavity at $x=x_1$ in a transverse spatial mode m and spin state s, propagating through the cavity by means of the Green function $\mathcal{G}$, and escaping at $x=x_2$ in a mode n with spin s'. The quantities $v_{n,m}$ denote the x component of the particle velocity in the modes n and m, respectively. Note that the spin-dependent Green function $\mathcal{G}$ is a 2×2 matrix.

The evaluation of the quantum-meachanical transmission probability (2) through microstructures of arbitrary shape (as shown in Fig. 1) requires an efficient numerical tool for solving the related transport equations. An adequate method is based on the use of a tight-binding Hamiltonian, equivalent to a real-space discretization of the Schrödinger equation, in combination with a recursive algorithm for computing the corresponding Green function, see, e.g., Refs. 29 and 30 and references therein. The advantages of the method arise from its flexibility: different geometries (and topologies) are readily handled, as well as the presence of magnetic fields or eventually disorder potentials which can be easily included or modified. During the last decade the method has nearly exclusively been used for the study of spin-independent transport.[31] In this paper we generalize this approach to account for spin-orbit scattering and for the coupling of the spin degree of freedom to inhomogeneous magnetic fields including nonadiabatic spin-flip processes.

We consider noninteracting electrons with spin described by the Pauli matrix vector $\vec{\sigma}$. The spin coupling to a magnetic field $\vec{B}=\vec{\nabla}\times\vec{A}_{\mathrm{em}}$ is accounted for by the Zeeman term $\mathcal{H}_s=\mu\vec{B}\cdot\vec{\sigma}$. Moreover, spin-dependent effects can arise in the absence of external magnetic fields as well: The Rashba interaction $\mathcal{H}_{so}=\alpha_R(\vec{\sigma}\times\vec{p})_z/\hbar=i\alpha_R(\sigma_y\partial/\partial x-\sigma_x\partial/\partial y)$ (Ref. 13) accounts for the spin-orbit coupling of strength α_R in the presence of a vertical electric field (in z direction). The corresponding general Hamiltonian (for electrons of charge $-e$) then reads[35]

$$\mathcal{H}=\frac{1}{2m^*}\left[\vec{p}+\frac{e}{c}\vec{A}_{\mathrm{em}}(\vec{r})\right]^2+V(\vec{r})+\mu\vec{B}(\vec{r})\cdot\vec{\sigma}+\frac{\alpha_R}{\hbar}\left[\vec{\sigma}\times\left(\vec{p}+\frac{e}{c}\vec{A}_{\mathrm{em}}(\vec{r})\right)\right]_z, \tag{3}$$

where $\mu=g^*\mu_B/2=g^*e\hbar/(4m_0c)$ is the magnetic moment, μ_B the Bohr magneton, m_0 the bare electron mass, m^* the effective electron mass, and g^* the effective material-dependent gyromagnetic ratio. The electrostatic potential $V(\vec{r})$ in Eq. (3) can represent, as in the present case, the confining potential of a 2D ballistic conductor (see Fig. 1) or a disorder potential.

After introducing a 2D square grid of spacing a (identifying $x\equiv ka$ and $y\equiv la$, with k,l integers) we discretize the dimensionless Schrödinger equation $(2m^*a^2/\hbar^2)(E-\mathcal{H})\Psi(\vec{r})=0$ corresponding to Eq. (3) for spinors

$$\Psi(\vec{r})=\begin{pmatrix}\Psi_1(\vec{r})\\ \Psi_2(\vec{r})\end{pmatrix}. \tag{4}$$

Employing $\vec{p}=-i\hbar\vec{\nabla}$ and chosing the grid for a given field strength B such that $Ba^2\ll\phi_0=hc/e$, we arrive at the tight-binding representation[36–38]

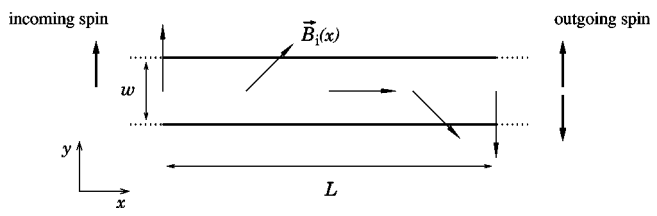

FIG. 2. Two-dimensional straight ballistic conductor of width w and length L subject to a rotating in-plane magnetic field $\vec{B}_i=B_i\sin[(\pi/L)x]\,\hat{x}+\cos[(\pi/L)x]\,\hat{y}$, which vanishes for $x<0$ and $x>L$. The spin orientation of incoming and outgoing channels is defined with respect to the y axis.

$$\tilde{\mathcal{H}} \equiv \frac{2m^*a^2}{\hbar^2}(E-\mathcal{H}) = \sum_{k,l} \left\{ \begin{pmatrix} \tilde{h}_{kl}^{11} & \tilde{h}_{kl}^{12} \\ \tilde{h}_{kl}^{21} & \tilde{h}_{kl}^{22} \end{pmatrix} |k,l\rangle\langle k,l| \right.$$
$$+ \left[\begin{pmatrix} \exp[i2\pi(aA_{\mathrm{em}}^{\mathrm{x}}/\phi_0)] & -\tilde{\alpha}_{\mathrm{R}}/2 \\ \tilde{\alpha}_{\mathrm{R}}/2 & \exp[i2\pi(aA_{\mathrm{em}}^{\mathrm{x}}/\phi_0)] \end{pmatrix} \right.$$
$$\left. \times |k,l\rangle\langle k+1,l| + \mathrm{H.c.} \right]$$
$$+ \left[\begin{pmatrix} \exp[i2\pi(aA_{\mathrm{em}}^{\mathrm{y}}/\phi_0)] & i\,\tilde{\alpha}_{\mathrm{R}}/2 \\ i\,\tilde{\alpha}_{\mathrm{R}}/2 & \exp[i2\pi(aA_{\mathrm{em}}^{\mathrm{y}}/\phi_0)] \end{pmatrix} \right.$$
$$\left. \left. \times |k,l\rangle\langle k,l+1| + \mathrm{H.c.} \right] \right\} \quad (5)$$

with

$$\tilde{h}_{kl}^{11} = \tilde{E} - \tilde{V} - 4 - \tilde{\mu}B_{\mathrm{z}},$$
$$\tilde{h}_{kl}^{12} = -\tilde{\mu}(B_{\mathrm{x}} - iB_{\mathrm{y}}) - \tilde{\alpha}_{\mathrm{R}} 2\pi a(A_{\mathrm{em}}^{\mathrm{y}} + iA_{\mathrm{em}}^{\mathrm{x}})/\phi_0,$$
$$\tilde{h}_{kl}^{21} = -\tilde{\mu}(B_{\mathrm{x}} + iB_{\mathrm{y}}) - \tilde{\alpha}_{\mathrm{R}} 2\pi a(A_{\mathrm{em}}^{\mathrm{y}} - iA_{\mathrm{em}}^{\mathrm{x}})/\phi_0,$$
$$\tilde{h}_{kl}^{22} = \tilde{E} - \tilde{V} - 4 + \tilde{\mu}B_{\mathrm{z}}.$$

Here we introduced the scaled parameters $\tilde{\mu} = (2m^*a^2/\hbar^2)\mu$, $\tilde{\alpha}_{\mathrm{R}} = (2m^*a/\hbar^2)\alpha_{\mathrm{R}}$, $\tilde{E} = (2m^*a^2/\hbar^2)E$, and $\tilde{V} = (2m^*a^2/\hbar^2)V$. Equation (5) shows that the consideration of the spin degree of freedom gives rise to generalized on-site and hopping energies represented by 2×2 matrices. The relative magnitude of the matrix elements determines, besides aspects related to the orbital motion, the spin dynamics of the carriers, generally leading to spin flips. We note that the Zeeman interaction $\tilde{\mu}B_{\mathrm{z}}$ does not enter into the hopping terms in Eq. (5) because the Zeeman term does not involve derivatives. For vanishing spin-orbit coupling [$\tilde{\alpha}_{\mathrm{R}} = 0$ in Eq. (5)] the hopping matrices are diagonal in spin space and only the on-site terms generate spin flips.

For the calculation of the spin-dependent Green-function matrix $\mathcal{G}$ we generalized the method used for spinless particles.[30] This is based on the Dyson equation,

$$\mathcal{G} = \mathcal{G}_0 + \mathcal{G}_0 U \mathcal{G} = \mathcal{G}_0 + \mathcal{G} U \mathcal{G}_0, \quad (6)$$

which relates the Green function $\mathcal{G}_0$ of the unperturbed system to the Green function $\mathcal{G}$ of the system under perturbation U. In the present case U is given by the hopping terms $|k,l\rangle\langle k+1,l|$ and $|k+1,l\rangle\langle k,l|$ in Eq. (5). Relation (6) represents an implicit equation for $\mathcal{G}$, leading to a system of equations which can be solved recursively.[29,36] A similar method has recently been used for the study of the spin-orbit coupling in quasiballistic and disordered wires.[33,34]

While the approach outlined above is rather general and applicable to spin transport in a variety of different systems, from now on we focus on pure Zeeman coupling in the presence of inhomogeneous magnetic fields, i.e., $\alpha_{\mathrm{R}} \equiv 0$ in the Hamiltonian (3). In addition, we consider ballistic (disorder free) dynamics. Apart from this purely numerical approach, corresponding analytical solutions have been obtained in the limit of 1D rings in paper I and.[20] We compare both results in Sec. IV B.

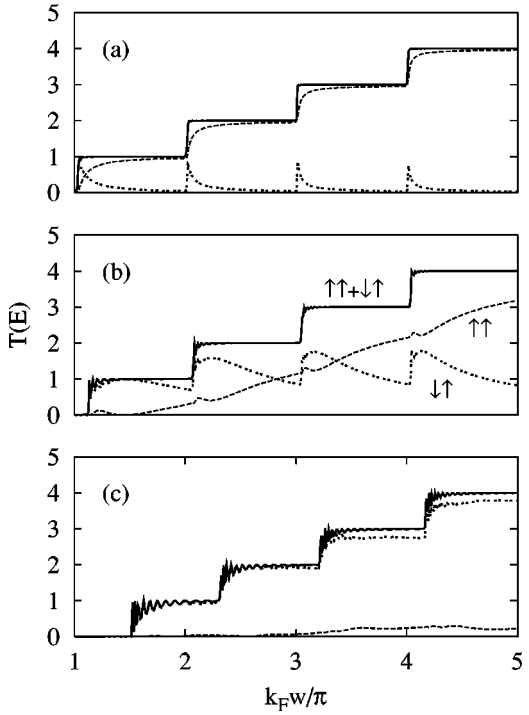

FIG. 3. Numerically calculated spin-dependent transmission through the straight 2D conductor of Fig. 2 using the generalized recursive Green function method introduced in Sec. II. Results are shown for the quantum transmission of incoming spin-up polarized particles (↑, defined with respect to the *y* axis, see Fig. 2) in the presence of a weak (a), moderate (b), and strong (c) magnetic field as a function of the dimensionless wave number $k_F w/\pi$. The overall transmission (solid line) is split into its components $T^{\uparrow\uparrow}$ (dashed line) and $T^{\downarrow\uparrow}$ (dotted line) corresponding to outgoing spin-up (↑) and spin-down (↓) channels, respectively.

III. CASE STUDY: QUANTUM WIRES

To illustrate our spin-dependent numerical approach and basic spin effects we consider first the simple geometry shown in Fig. 2. It consists of a straight ballistic conductor of width w and length L in a rotating in-plane magnetic field of the form $\vec{B}_{\mathrm{i}} = B_{\mathrm{i}}\{\sin[(\pi/L)x]\,\hat{x} + \cos[(\pi/L)x]\,\hat{y}\}$, which vanishes at leads for $x<0$ and $x>L$. Chosing a proper gauge, the x and y components of the vector potential $\vec{A}_{\mathrm{em}}$ generating the field $\vec{B}_{\mathrm{i}}$ vanish in the plane $z=0$.[39] Moreover, as depicted in Fig. 2, we consider asymptotic spin states defined with respect to the y axis, namely, eigenvectors of σ_{y}.

Our numerical results are summarized in Fig. 3. It shows the quantum transmission of incoming spin-up electrons (↑) in the presence of a weak (a), moderate (b), and strong (c) magnetic field as a function of the dimensionless wave number $k_F w/\pi$. The overall transmission (solid line) is decomposed into its components $T^{\uparrow\uparrow}$ (dashed line) and $T^{\downarrow\uparrow}$ (dotted

line) corresponding to outgoing up- (↑) and down-polarized (↓) spin channels, respectively.

For spinless transport, the conductance through the 2D wire of Fig. 2 is quantized as for a quantum point contact.[40] The conductance exhibits steps of size $\Delta G = 2e^2/h$ equivalent to steps $\Delta T = 1$ in the transmission, each time a new transverse mode is opened in the conductor. In the presence of the magnetic field $\vec{B}_\mathrm{i}$, the overall transmission $T^{\uparrow\uparrow} + T^{\downarrow\uparrow}$ [solid line in Figs. 3(a)–3(c)] shows the same steps, up to small deviations for strong B_i. However, the individual spin components vary considerably as the field strength B_i increases [from (a) to (c)]. The relative strength of the field B_i can be characterized by comparing the relevant time scales in the system,[20–24,32,36] i.e. the Larmor frequency $\omega_\mathrm{s} = 2\mu B_\mathrm{i}/\hbar$ of spin precession around the local field with the characteristic frequency $\omega \sim v/L$ of orbital motion (with velocity v) in the region where the direction of the field changes significatively.[41]

In the weak-field limit ($\omega \gg \omega_\mathrm{s}$) the spin dynamics is slow compared to the orbital motion. In this situation the *nonadiabatic* channel $T^{\uparrow\uparrow}$ [dashed line in Fig. 3(a)] dominates the transport, and most electrons leave the conductor conserving the incoming spin-up polarization. The opposite limit of a strong field is given when $\omega \ll \omega_\mathrm{s}$. Here the spin stays *adiabatically* aligned with the spatially varying magnetic field direction during transport, such that the spin orientation is finally reversed at the outgoing lead: the particles escape in spin-down state after traveling through the conductor, and the main contribution to the transmission is given by $T^{\downarrow\uparrow}$ [dotted line in Fig. 3(c)]. We thus refer to $T^{\downarrow\uparrow}$ and $T^{\uparrow\uparrow}$ as the adiabatic and nonadiabatic transmission channels, respectively. For the intermediate case of moderate fields, $\omega \sim \omega_\mathrm{s}$, Fig. 3(b), the contribution of both adiabatic and nonadiabatic channels is comparable. Moreover, there is further structure in the quantum transmission which we discuss in the following.

(i) The adiabatic channel $T^{\downarrow\uparrow}$ is enhanced each time a new transverse mode opens, see dotted lines in Figs. 3(a) and 3(b). This is related to the fact that different modes propagate with different velocities $v_x(n)$ along the x direction, and the mode specific orbital frequency $\omega = \omega_n = v_x(n)/L$ has to be compared with ω_s in order to determine whether the corresponding spin propagates adiabatically or not.[42] When a new mode just opens, the associated particle velocity v_x vanishes, leading to a small ω and thereby giving rise to a large adiabatic contribution.

(ii) The staircase profile of the overall transmission in Fig. 3 is shifted to higher values of $k_F w/\pi$ (corresponding to higher Fermi energies for the incoming electrons) as B_i increases from Figs. 3(a) to 3(c). This is due to a Zeeman *barrier* which the incoming spin-up electrons must overcome in the adiabatic limit of strong field. Incoming spin-down electrons experience a Zeeman *well* which does not lead to such a shift. (In Fig. 3 only spin-up polarized electrons are shown.)

(iii) We observe an oscillatory pattern modulating the plateaus in the overall transmission (solid line) as the adiabatic limit is approached [Fig. 3(c) in particular]. This is also a consequence of the Zeeman barrier, giving rise to interfering backscattered waves, similar to the textbook case of a wave scattered at a 1D rectangular potential barrier.

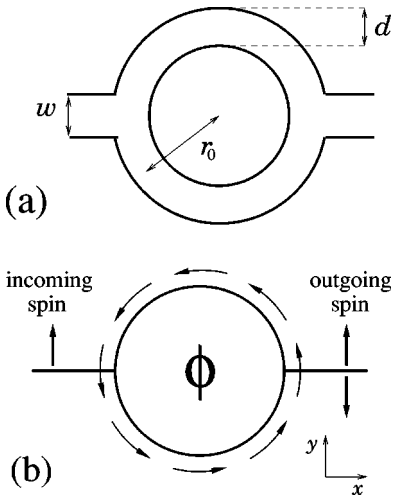

FIG. 4. Geometries of ballistic microstructures used in the quantum calculations of the spin-dependent conductance for a circular (in plane) magnetic field texture $\vec{B}_\mathrm{i}$, Eq. (7), plus a magnetic flux ϕ. Spin directions are defined with respect to the y axis.

We finally point out that for the simple geometry of Fig. 2 Berry phases[14] arising in the adiabatic limit do not play a role in the conductance because their observation requires doubly connected geometries.[20,32,43] However, the introduction of disorder could lead to signatures of Berry phases in the magnetoconductance via the suppression of weak localization.[44]

IV. FROM DIABATIC TO ADIABATIC SPIN TRANSPORT IN MESOSCOPIC RINGS

The above discussion of spin transport through a straight wire geometry illustrated basic spin-dependent transport phenomena. Here we discuss more sophisticated spin-dependent effects arising in transport of unpolarized electrons through mesoscopic ring geometries subject to different field textures.

A. Magnetic field setup

We consider ballistic ring structures with two attached leads (see Fig. 4) subject to a magnetic field which has two contributions, $\vec{B}(\vec{r}) = \vec{B}_0 + \vec{B}_\mathrm{i}(\vec{r})$. The first term corresponds to a perpendicular uniform magnetic field $\vec{B}_0 = B_0\hat{z}$ leading to a magnetic flux $\phi = \pi r_0^2 B_0$ (where r_0 is the mean radius of the ring) to be used as a tunable parameter to study the magnetoconductance of the microstructures. The second contribution to $\vec{B}(\vec{r})$ is given by circular in-plane field [see Fig.4(b)] reading in polar coordinates

$$\vec{B}_\mathrm{i}(\vec{r}) = B_\mathrm{i}(r)\,\hat{\varphi} = \frac{a}{r}\ \hat{\varphi}. \tag{7}$$

Such a field can be viewed as being generated by a perpendicular electrical current I through the center of the micro-

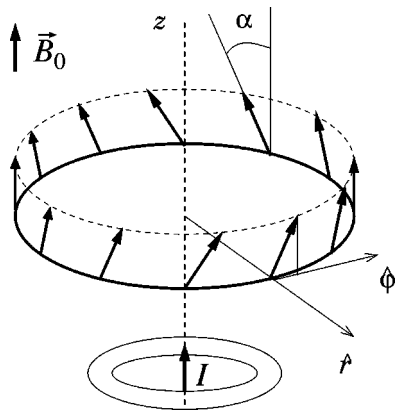

FIG. 5. Magnetic-field texture corresponding to a circular field generated by an electric current I along the z axis [Eq. (7)] plus an additional uniform field $\vec{B}_0 = B_0\,\hat{z}$, defining a tilt angle α. The field is evaluated on a one-dimensional ring contour.

structure with $a = \mu^* I/2\pi$.[45] The configuration of the overall magnetic field is schematicaly represented in Fig. 5.

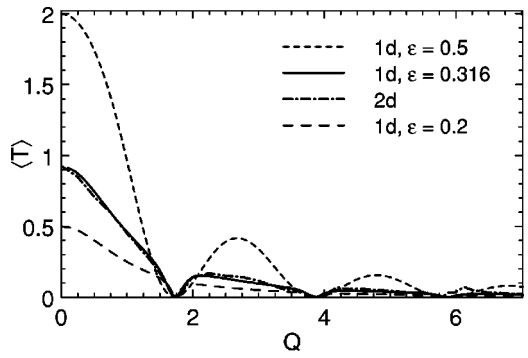

FIG. 6. Spin-dependent quantum transmission of unpolarized electrons through a 1D ring calculated within the transfer-matrix approach of paper I. The inhomogeneous magnetic field lies in the plane of the ring, see Fig. 4. The energy-averaged transmission $\langle T \rangle$ as a function of the adiabaticity parameter Q is shown for coupling parameters $\epsilon = 0.2$, 0.316, 0.5 and $\phi = 0$. The numerical result of the 2D tight-binding approach for a ring with one open channel is given by the dashed-dotted line and follows closely the curve for $\epsilon = 0.316$.

B. Comparison between analytical and numerical results

We begin our analysis of the spin-dependent conductance through mesoscopic rings by comparing numerical results for 2D rings, based on the technique described in Sec. II, with results for 1D rings derived in paper I.[1] To this end, we consider the spin-dependent transmission of unpolarized electrons in the entire crossover regime between zero magnetic field (diabatic limit, $B_i = 0$) and the adiabatic limit (B_i large). We quantify the degree of adiabaticity in terms of the parameter

$$Q \equiv \omega_s / \omega, \tag{8}$$

the ratio between the spin precession frequency ω_s and the orbital frequency ω. Hence, Q increases as adiabaticity is approached.

The numerical quantum-mechanical result for the energy-averaged conductance in a quasi-1D ring, i.e., a 2D ring with just one open channel, as a function of Q is shown as the dashed-dotted line in Fig. 6. It exhibits an overall Lorentzian decay[24] and distinct zeros for certain field strengths.

These features can be well understood within a complementary 1D model built from a (strictly) 1D ballistic ring coupled to 1D leads. In this case, the Schrödinger equation for the Hamiltonian (3) can be solved exactly for all values of the adiabaticity parameter Q [if $V(\vec{r}) = 0$], see paper I (Ref. 1) of this series for details and references. In short, the 1D model in paper I employs a transfer-matrix approach to describe transport properties, making use of the exact eigenstates of the 1D Hamiltonian. The coupling between the leads and the 1D ring is specified by a scattering matrix with coupling constant ϵ as parameter. Zero and strongest coupling is described by $\epsilon = 0$ and $\epsilon = 0.5$, respectively.

As an example we show in Fig. 6 results for the energy-averaged transmission probability $\langle T(Q,\epsilon) \rangle$ in the case of a circular in-plane magnetic field ($\alpha = \pi/2$) with Aharonov-Bohm flux $\phi = 0$. The transmission vanishes in the adiabatic limit ($Q \to \infty$) due to the presence of a Berry phase that leads to an additional phase shift. Its action can be interpreted as a geometric flux[32] of half a flux quantum acting similar to an Aharonov-Bohm flux. Hence, for $\phi = 0$ the additional Berry phase causes destructive interference of the waves in the two arms of the ring, leading to a vanishing transmission. We refer the interested reader to the detailed discussion in paper I.

In paper I it is also shown that the energy-averaged transmission vanishes due to destructive interference at points $Q = \sqrt{4m^2 - 1}$ with integer m, i.e., $Q = \sqrt{3}, \sqrt{15}, \ldots$, in agreement with the zeros observed in Fig. 6. This gives rise to the observed oscillating structure of the averaged transmission probability $\langle T \rangle$ and holds for all coupling strengths ϵ, see Fig. 7 in paper I. Hence, tuning Q (i.e., the strength of the inhomogeneous field) enables for controlling the overall conductance via the coupling of the electron spin to the field.

While the coupling parameter ϵ appears naturally in the analytical transfer-matrix approach in paper I, an effective ϵ is difficult to determine from the 2D tight-binding calculations described in Sec. II. We have used the quasi-1D tight-binding transmission at $Q = 0$ to fix the parameter ϵ to 0.316 in the transfer-matrix approach. This choice yields considerable agreement between the quasi-1D numerical and 1D analytical curves in the whole Q regime, see Fig. 6. We further note that in an experimental setup the effective coupling ϵ could be controlled by means of local gates acting as tunable potential barriers at the junctions.

V. MAGNETOCONDUCTANCE OF SPIN-POLARIZED CURRENTS

In the following we show how the transmission and polarization of *spin-polarized* electrons in various ring geometries can be affected by an additional magnetic flux $\phi = \pi r_0^2 B_0$. Numerical results for single and multichannel

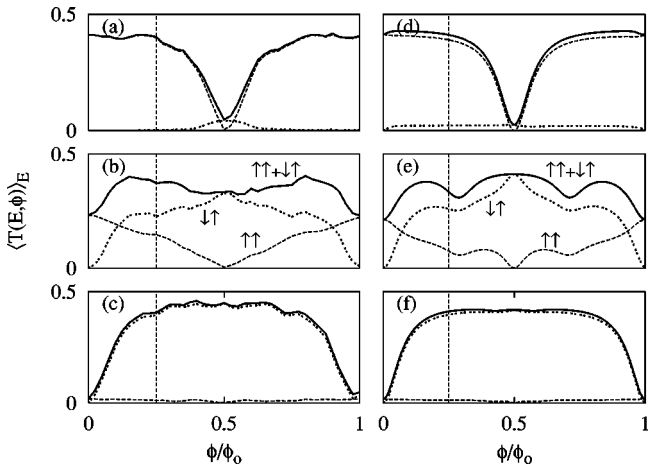

FIG. 7. Energy-averaged transmission of spin-up polarized electrons (spin in y direction, see text) through a quasi-1D ring as a function of a flux $\phi=\pi r_0^2 B_0$ in the presence of a circular in-plane field $B_i \gg B_0$ of increasing strength: (a) weak ($Q\approx 0.05$), (b) moderate ($Q\approx 0.7$), (c) strong ($Q\approx 4$). The overall transmission (solid line) is split into its components $\langle T^{\uparrow\uparrow}\rangle$ (dashed) and $\langle T^{\downarrow\uparrow}\rangle$ (dotted). Note the change in the polarization upon tuning the flux and particularly the spin-switching mechanism at $\phi=\phi_0/2$. Panels (d)–(f) show corresponding calculations for a strictly 1D ring using the transfer-matrix approach (paper I) with coupling constant $\epsilon=0.3$. These are to be compared with panels (a)–(c), respectively. Equivalent results are obtained for spin-down electrons (not shown here).

transport are presented and discussed. Different ring geometries and field textures are considered.

A. Aharonov-Bohm ring as a spin switch

We consider transport of spin-up polarized electrons through a quasi-1D ring, Fig. 4(a), in the presence of the circular in-plane field $\vec{B}_i$ given by Eq. (7). The spin orientation is defined with respect to the y axis as shown in Fig. 4(b). For the conductance calculations we apply the numerical method outlined in Sec. II and compare with 1D results from paper I. To this end we focus on the case where leads and ring support only one open channel and choose the field configuration as quasi-in-plane texture where $B_0 \ll B_i$. The aspect ratio of the ring is $d/r_0=0.25$. Our numerical results for the energy-averaged transmission $\langle T(E,\phi)\rangle_E$ are shown in Figs. 7(a)–7(c) for three different scaled strengths $Q=\omega_s/\omega$ of the in-plane inhomogeneous field ($Q\ll 1$; $Q\sim 1$; $Q\gg 1$). In the weak-field limit [$Q\ll 1$, Fig. 7(a)], the electron spin is barely affected by the magnetic field. The total transmission (solid line) shows the usual AB oscillations and is predominantly given by $\langle T^{\uparrow\uparrow}\rangle$ (dashed line), whereas $\langle T^{\downarrow\uparrow}\rangle$ (dotted line) is close to zero. The behavior is reversed in the adiabatic limit, Fig. 7(c), where the spin-flip coefficient $\langle T^{\downarrow\uparrow}\rangle$ carries the AB oscillations, now shifted by $\phi_0/2$ due to the geometrical phase as discussed in Refs. 24 and 32, and $\langle T^{\uparrow\uparrow}\rangle$ is, in turn, nearly zero.

Figure 7(b) shows the general case of an intermediate field ($Q\sim 1$). With increasing flux the polarization of transmitted electrons changes continuously. Most interestingly, $\langle T^{\downarrow\uparrow}\rangle=0$ at $\phi=0$, while $\langle T^{\uparrow\uparrow}\rangle=0$ for $\phi=\phi_0/2$. This means that for zero flux an ensemble of spin-polarized charge carriers is transmitted keeping the incoming spin direction (spin-flip suppression), while at $\phi=\phi_0/2$ the transmitted electrons just reverse their spin direction. In other words, by tuning the flux from 0 to $\phi_0/2$, one can reverse the polarization of transmitted particles in a controlled way. Hence, the AB ring combined with the rotationally symmetric magnetic field acts as a tunable spin switch. This mechanism proves to be *independent* of the field strength B_i or Q, which determines only the size of the spin-reversed current. Alternatively, for a fixed flux $0<\phi<\phi_0/2$ (vertical dashed line in Fig. 7) the spin polarization is reversed upon passing from the nonadiabatic to the adiabatic regime, while the total transmission remains nearly constant.

The mechanism for changing the spin direction does neither rely on the spin coupling to the control field B_0 (as long as $B_0 \ll B_i$), nor on the Zeeman splitting often exploited in spin filters.[8,47] The effect exists for both spin-up and spin-down polarized particles.[36] It is of pure quantum interference origin, due to a cooperation between charge (which couples to the flux ϕ) and spin (which couples to the field $\vec{B}_i$) coherence, and exists not only for the smoothed energy-averaged transmission as shown in Fig. 7 but also for the transmission at a given energy.

We further note that the spin coupling to the inhomogeneous field produces an attenuation of the AB oscillations in the overall transmission for moderate fields, confirm Fig. 7(b). This is due to the comparable amplitude of the $\phi_0/2$-shifted components $\langle T^{\uparrow\uparrow}\rangle$ and $\langle T^{\downarrow\uparrow}\rangle$.

Corresponding calculations for strictly 1D rings using the transfer-matrix approach (paper I) lead to similar results. They are summarized in Figs. 7(d)–7(f), to be compared with the above discussed results of Figs. 7(a)–7(c), respectively.

B. Necessary conditions for the spin-switching mechanism

For a strictly 1D ring an analytical proof for the spin-switch effect is given in paper I. There we show rigorously that the transmission coefficient $T^{\uparrow\uparrow}$ vanishes completely at $\phi=\phi_0/2$, if the magnetic field to which the spins couple has no component perpendicular to the plane of the ring. In the following we explore the range of validity of the spin-switch effect discussed in Sec. V A. To this end, we consider a set of five alternative situations and generalizations with respect to the previous case of a single-channel symmetric ring.

(I) To clarify whether the effect pertains for more general geometries than a 1D ring, we study transport through a doubly connected 2D cavity, a Sinai-type billiard as shown in Fig. 8. This geometry still obeys reflection symmetry with respect to the horizontal ($x-$) axis, but not necessarily with respect to the vertical axis. Numerical calculations are performed for leads supporting only one open channel. However, within the cavity the number of open modes is larger and not well defined, since the system is not separable. In Fig. 9 results are displayed for the energy-averaged transmission $\langle T(E,\phi)\rangle_E$, again for incoming spin-up polarized particles, in the presence of a weak (a), moderate (b), and strong (c) inhomogeneous in-plane field. The general features are

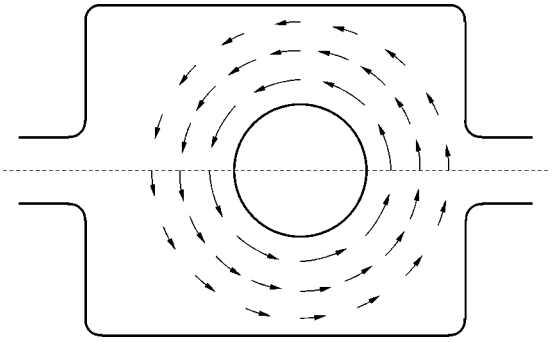

FIG. 8. Ring-type geometry with a horizontal symmetry axis used for the numerical calculations shown in Fig. 9. The circular in-plane field $\vec{B}_i$, Eq. (7), has its origin at the center of the inner disk.

similar to those observed in the quasi-1D and 1D cases (Fig. 7). However, some deviations appear. While the spin-flip suppression $\langle T^{\downarrow\uparrow}\rangle = 0$ remains true for $\phi = 0$, the component $\langle T^{\uparrow\uparrow}\rangle$ does not vanish completely at $\phi = \phi_0/2$, even though it still exhibits a pronounced minimum [panel (b)]. This is a consequence of the comparatively large fraction of the total magnetic flux penetrating the accessible region of the Sinai cavity in Fig. 8, giving rise to a whole range of ''path-dependent'' accumulated fluxes. Consequently, the point $\phi = \phi_0/2$ is no longer well defined. We further note that, owing

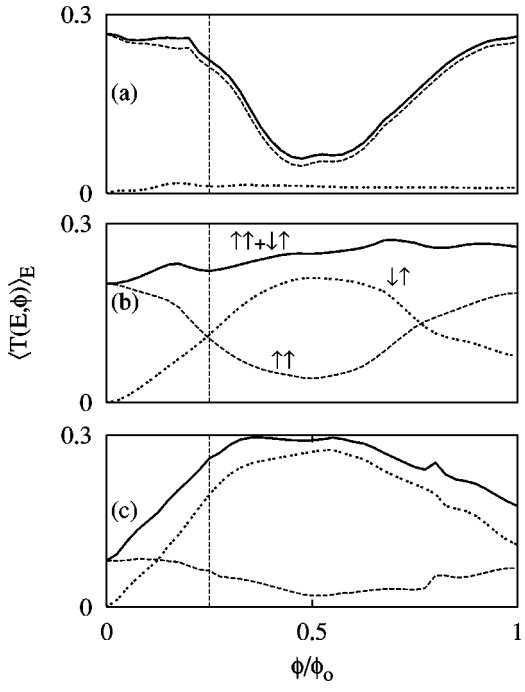

FIG. 9. Averaged transmission for spin-up polarized incoming electrons through the 2D ringwise geometry of Fig. 8 as a function of the mean flux $\phi = \pi r_0^2 B_0$ in the presence of a circular in-plane field $B_i \gg B_0$ of increasing strength: (a) weak, (b) moderate, (c) strong. The overall transmission (solid line) is split into its components $\langle T^{\uparrow\uparrow}\rangle$ (dashed) and $\langle T^{\downarrow\uparrow}\rangle$ (dotted). Note that the spin-switching mechanism at $\phi = \phi_0/2$ is attenuated with respect to Fig. 7 (due to the large effective area of the inner cavity in Fig. 8, see text) but still present.

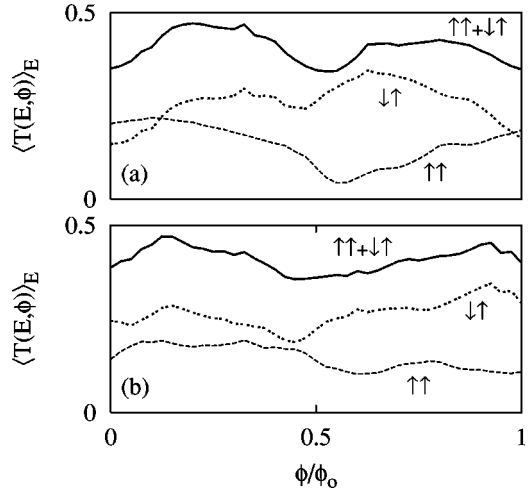

FIG. 10. Averaged transmission for spin-up polarized incoming electrons through a quasi-1D ring with slightly asymmetric arms, see text. The parameters defining the asymmetry via a vertical displacement of the inner disk are (a) $\Delta_y/d = 0.05$ and (b) $\Delta_y/d = 0.10$. A moderate inhomogeneous field strength, equivalent to that of Fig. 7(b), is applied. Note the absence of the spin-switching effect in panel (b).

to the appearence of Berry phases as in the quasi-1D case, the AB oscillations of $\langle T\rangle$ in Fig. 9 (solid line) show again a phase shift of $\phi_0/2$ near the adiabatic limit, panel (c), with respect to the weak-field limit, panel (a).

We conclude that despite relaxing the constraints of (i) the vertical reflection symmetry and (ii) the quasi-1D nature of the ring geometry, the spin-switch mechanism remains as an outstanding effect for a rather general class of doubly connected geometries.

(II) To investigate the role of the remaining horizontal reflection symmetry we slightly shift the central disk of the symmetric ring in Fig. 4(a) by an amount Δ_y along the y direction, while keeping all other parameters as in Figs. 7(a)–7(c). This leads to a difference in the effective lengths of paths along the upper and lower arms, breaking the horizontal reflection symmetry. Numerical results for a moderate field strength [as in Fig. 7(b)] are shown in Figs. 10(a) and 10(b) for a scaled shift $\Delta_y/d = 0.05$ and $\Delta_y/d = 0.10$, respectively. In contrast to the symmetric case of Fig. 7(b), both panels depict spin flips ($\langle T^{\downarrow\uparrow}\rangle \neq 0$) already at $\phi = 0$. Nevertheless, for the smaller asymmetry in panel (a) a distinct modulation of the spin-dependent components $\langle T^{\uparrow\uparrow}\rangle$ and $\langle T^{\downarrow\uparrow}\rangle$ as a function of ϕ is observed, and a spin-reversed current $\langle T^{\downarrow\uparrow}\rangle$ prevails near $\phi = \phi_0/2$. With increasing deformation parameter Δ_y the spin-switch effect is disappearing as seen from Fig. 10(b).

As a result we find that reflection symmetry with respect to the axis defined by the two opposite leads is required for spin-flip suppression at $\phi = 0$ and spin inversion at $\phi = \phi_0/2$.

(III) In the following we return to the symmetric ring, but relax the constraint $B_0 \ll B_i$ of the in-plane field configuration. We consider an inhomogeneous field B_i of moderate strength such that $B_i \sim B_0$ at $\phi = \phi_0/2$. As a consequence, the overall field texture is characterized by a finite tilt angle α

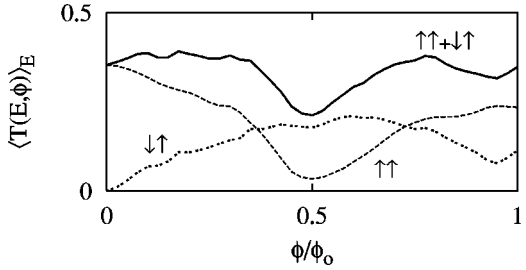

FIG. 11. Averaged transmission for geometry, field strength and asymptotic spin states equivalent to those of Fig. 7(b), this time for comparable fields $B_i \sim B_0$ at $\phi = \phi_0/2$ (field texture displayed in Fig. 5). The spin coupling with the field B_0 generating the flux is not negligible.

$\neq \pi/2$ as displayed in Fig. 5. Numerical results for single-channel transmission of incoming spin-up particles are shown in Fig. 11. Although no longer perfect, spin switching still takes place near $\phi = \phi_0/2$. Thus, the spin-coupling to the field generating the flux which is not negligible in this case, produces an attenuation of the effect with respect to in-plane field result; the overall effect, however, still persists. This is similar to the result found in Fig. 9(b) for a ring-type geometry with large aspect ratio (Fig. 8). In the remaining part of the paper we return to the situation of a quasi-in-plane field, $B_0 \ll B_i$.

(IV) So far the spin-switching mechanism has been considered for asymptotic spin states polarized in the in plane $\pm y$ direction, i.e., for eigenvectors of the Pauli matrix σ_y. In order to see whether the effect depends on the polarization direction with respect to the field texture, we introduce asymptotic spin states orientated along the z axis perpendicular to the 2D system, i.e., eigenvectors of σ_z. The transmission amplitudes between z-orientated asymptotic spin states, $t^{s_z' s_z}$, are a linear combination of those defined along the y axis, $t^{s_y' s_y}$. Numerical results for corresponding spin-up electrons are displayed in Fig. 12 for a symmetric quasi-1D ring in the presence of a weak (a), moderate (b), and strong (c) in-plane inhomogeneous field [same parameters as in Figs. 7(a)–7(c)]. In the weak-field limit, Fig. 12(a), the component $\langle T^{(\downarrow\uparrow)_z} \rangle$ (dotted line) is close to zero, and the total transmission (solid line) shows AB oscillations predominantly given by $\langle T^{(\uparrow\uparrow)_z} \rangle$ (dashed line) as expected. In the opposite strong-field (adiabatic) limit, Fig. 12(c), the AB oscillations exhibit a phase shift of $\phi_0/2$ due to geometrical phases. The spin polarization of transmitted particles, however, is not reversed as in the case of incoming y-polarized spins [Fig. 7(c)]. On the contrary, the coefficients $\langle T^{(\uparrow\uparrow)_z} \rangle$ and $\langle T^{(\downarrow\uparrow)_z} \rangle$ have similar phase and magnitude, leading to randomization of the orientation of transmitted spins. This is a consequence of the spin precession taking place around the local field direction during transport in the adiabatic limit.[48] For moderate field strengths, Fig. 12(b), no pronounced spin-switching mechanism appears either, though the spin-reversed component $\langle T^{(\downarrow\uparrow)_z} \rangle$ is maximum at $\phi = \phi_0/2$. A spin-flip suppression remains at $\phi = 0$ independent of B_i.

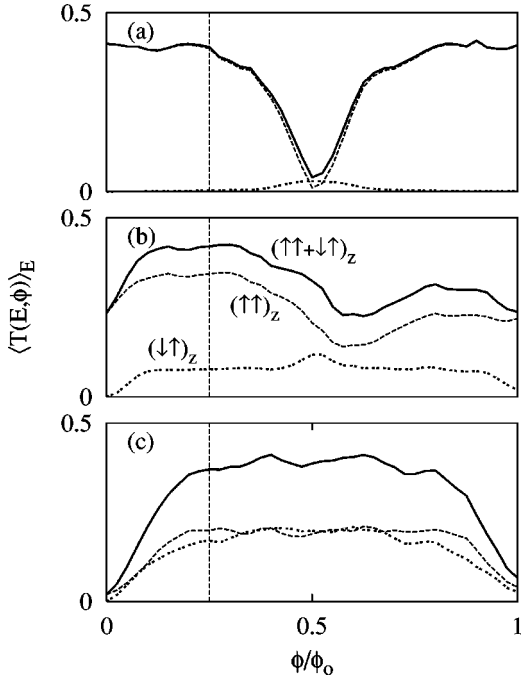

FIG. 12. Averaged transmission in the in-plane case ($B_i \gg B_0$), geometry and field strengths equivalent to those of Figs. 7(a)–(c), but for asymptotic spin-states defined with respect to the z axis.

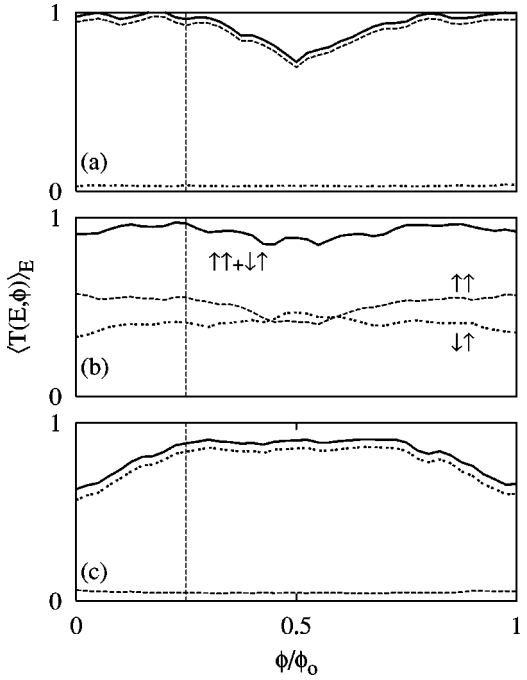

FIG. 13. Multichannel averaged transmission as function of a flux $\phi = \pi r_0^2 B_0$ for incoming electrons in spin-up states (oriented along the y direction) traversing a symmetric ring structure [Fig. 4(a)] in the presence of a circular in-plane field $B_i \gg B_0$ of increasing strength: (a) weak, (b) moderate, (c) strong. The overall transmission (solid line) is split into its components $\langle T^{\uparrow\uparrow} \rangle = \Sigma_{n,m}^N \langle T_{nm}^{\uparrow\uparrow} \rangle$ (dashed) and $\langle T^{\downarrow\uparrow} \rangle = \Sigma_{n,m}^N \langle T_{nm}^{\downarrow\uparrow} \rangle$ (dotted) with $N = 2$ (see text).

(V) Finally we consider the case of *multichannel* transport, namely, leads of width w supporting more than one open channel ($N = \mathrm{Int}[k_F w/\pi] > 1$). Consequently, the spin-

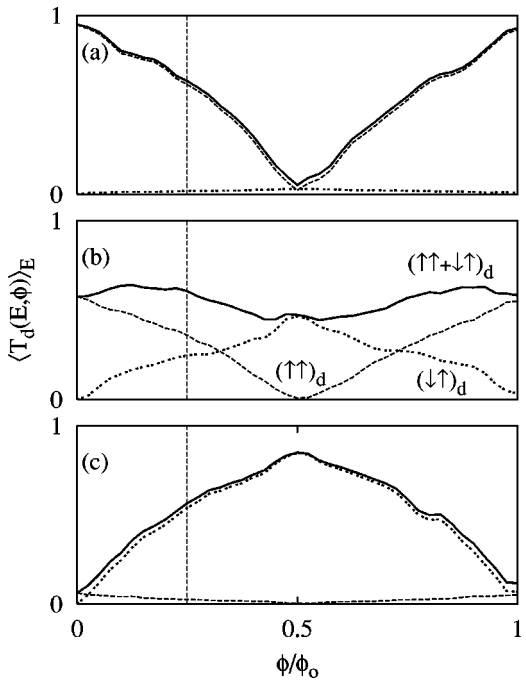

FIG. 14. Diagonal contribution (in mode number) to the multichannel averaged tranmission of Fig. 13. The overall diagonal transmission $\langle T_d\rangle$ (solid line) is split into its components $\langle T_d^{\uparrow\uparrow}\rangle = \langle T_{11}^{\uparrow\uparrow}\rangle + \langle T_{22}^{\uparrow\uparrow}\rangle$ (dashed) and $\langle T_d^{\downarrow\uparrow}\rangle = \langle T_{11}^{\downarrow\uparrow}\rangle + \langle T_{22}^{\downarrow\uparrow}\rangle$ (dotted). Note the similarity with the results of Fig. 7.

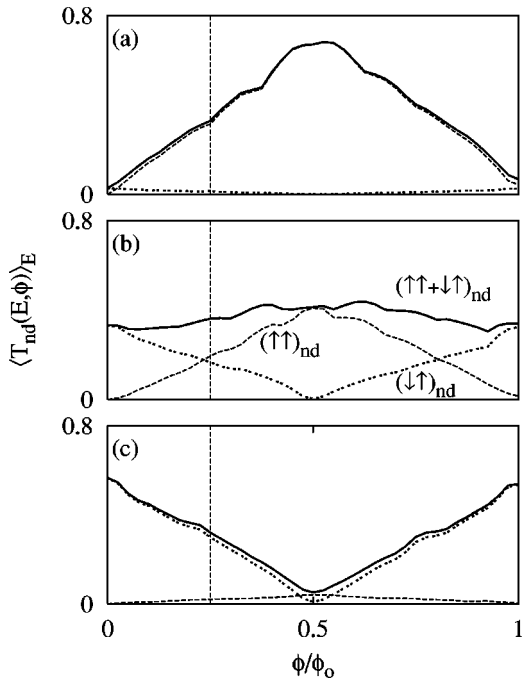

FIG. 15. Off-diagonal contribution (in mode number) to the multichannel averaged tranmission of Fig. 13. The overall off-diagonal transmission $\langle T_{nd}\rangle$ (solid line) is split into its components $\langle T_{nd}^{\uparrow\uparrow}\rangle = \langle T_{12}^{\uparrow\uparrow}\rangle + \langle T_{21}^{\uparrow\uparrow}\rangle$ (dashed) and $\langle T_{nd}^{\downarrow\uparrow}\rangle = \langle T_{12}^{\downarrow\uparrow}\rangle + \langle T_{21}^{\downarrow\uparrow}\rangle$ (dotted). Note the contrast with the complementary diagonal contribution in Fig. 14.

dependent transmission coefficients $T^{s's}$ consist now of a sum over incoming (m) and outgoing (n) modes $T^{s's} = \Sigma_{n,m}^{N} T_{nm}^{s's}$, see Eq. (1). Without loss of generality, we discuss here the case $N=2$ and return to our earlier definition of asymptotic spin states as eigenvectors of σ_y. Figure 13 shows numerical results for the total transmission of incoming spin-up polarized charge carriers through a symmetric ring as illustrated in Fig. 4(a). (The geometry parameters are equivalent to those used for the calculations in Figs. 7(a)–7(c); the energy average is taken between the (open) second and (still closed) third channel. The different panels correspond to a weak (a), moderate (b), and strong (c) inhomogeneous in-plane field. As expected, the main contribution to the total transmission (solid lines) in the weak field limit, given by $\langle T^{\uparrow\uparrow}\rangle$ [dashed line in panel (a)], is replaced by $\langle T^{\downarrow\uparrow}\rangle$ [dotted line in panel (c)] when the adiabatic limit is approached. Simultaneously, the AB oscillations are shifted due to geometrical phases. Furthermore, we no longer observe both spin-flip suppression at $\phi=0$ ($\langle T^{\downarrow\uparrow}\rangle \neq 0$) and polarization inversion at $\phi=\phi_0/2$ ($\langle T^{\uparrow\uparrow}\rangle \neq 0$) for moderate field strengths in panel (b).

Additional insight is gained by analyzing the respective contributions of the different current carrying transverse modes in the leads. Consider the transmission coefficients diagonal and nondiagonal in channel number, namely, $T_d^{s's} \equiv T_{11}^{s's} + T_{22}^{s's}$ and $T_{nd}^{s's} \equiv T_{12}^{s's} + T_{21}^{s's}$. The corresponding energy-averaged quantities are shown in Figs. 14 and 15, respectively. The results are organized as in Fig. 13. The traces in Fig. 14 show on the one hand that the diagonal term $\langle T_d\rangle$ exhibits the same features as for single-channel transport, see Fig. 7, including the spin-switch mechanism. On the other hand, we observe precisely the opposite behavior for the off-diagonal component $\langle T_{nd}\rangle$ in Fig. 15. This implies for zero flux that an ensemble of incoming polarized spins within, e.g., the first channel $m=1$ is partially transmitted keeping the original spin polarization only within the first outgoing channel $n=1$. At the same time, a complementary spin-reversed fraction of particles is leaving the cavity through the second outgoing channel, $n=2$. For flux $\phi=\phi_0/2$, the spin-reversed fraction exits the system through the lowest mode $n=1$, while the spins keep the original orientation within the second mode, $n=2$. In other words, by tuning ϕ from 0 to $\phi_0/2$ one can control, although not independently, the spin polarization of each outgoing channel provided that the incoming electrons were spin polarized. Furthermore, we point out that for $\phi=0$ the spin coupling to a finite in-plane field leads to nonzero (odd) cross terms in channel number. This is remarkable, since such cross terms do not contribute to the transmission of particles without spin for systems with horizontal reflection symmetry [see, e.g., the weak field limit of Fig. 15(a) at $\phi=0$].

We close by mentioning that the amplitude of the AB oscillations in the total transmission for weak fields, solid line in Fig. 13(a), is relatively small compared with its diagonal component, Fig. 14(a). This reflects the counteracting role played by the off-diagonal contribution [Fig. 15(a)] in the total transmission.

VI. SUMMARY AND CONCLUSION

We have studied nonadiabatic spin-dependent transport through ballistic conductors of different shape (straight and ring-type geometries) subject to inhomogeneous magnetic fields of varying strength. Our account generalizes studies of the regime of adiabatic spin-transport, widely discussed in the literature.[14,20,32,43] This regime is included here as the strong field limit.

For straight conductors we discussed several spin effects in the quantized conductance. In particular, we found a strong enhancement of the adiabatic spin channel each time a new transverse mode opens in the conductor, owing to the fact that electrons propagate slowly within the channel corresponding to the new mode.

For ring geometries we obtain numerically the explicit dependence of the transmission on the scaled field strength Q, which acts as an adiabaticity parameter, elucidating the role of geometrical phases in ballistic quantum transport and possible experimental realizations. Moreover, for in-plane field configurations and symmetric ballistic ring microstructures we demonstrate how an additional small flux ϕ can be used to control the spin dynamics and thereby tune the polarization of transmitted electrons.[24] This quantum mechanism, which is analytically investigated in detail in the preceding paper[1] does not require adiabaticity. We have also assessed in detail the range of validity of the spin-switch effect for various different situations relaxing constraints on symmetry, field configuration, and channel number. In combination with a spin detector such a device may be used to control spin polarized current, similar to the spin field-effect transistor proposed in Ref. 3. For metallic, generally diffusive conductors disorder breaks the spatial symmetry. We found numerically that the spin switch mechanism no longer prevails for diffusive rings.[49]

Finally, we point out that ballistic rings with Rashba (spin orbit) interaction, yielding an effective in-plane magnetic field in the presence of a vertical electric field, exhibit a similar spin-switch effect.[50]

ACKNOWLEDGMENTS

A larger part of this work was performed at the *Max-Planck-Institut for the Physics of Complex Systems* in Dresden, Germany. We thank the institute and particularly P. Fulde for continuous support. We gratefully acknowledge financial support from the *Alexander von Humboldt Foundation* and the *Deutsche Forschungsgemeinschaft* through the research group Ferromagnet-Semiconductor Nanostructures. We also thank J. Fabian, H. Schomerus, and D. Weiss for many useful discussions.

*Present address: NEST-INFM & Scuola Normale Superiore, 56126 Pisa, Italy.

[1] M. Hentschel, H. Schomerus, D. Frustaglia, and K. Richter, preceding paper, Phys. Rev. B **69**, 155326 (2004). First paper in the present series, referred to as paper I throughout the text.

[2] Y. Aharonov and D. Bohm, Phys. Rev. **115**, 485 (1959).

[3] S. Datta and B. Das, Appl. Phys. Lett. **56**, 665 (1990).

[4] G.A. Prinz, Science **282**, 1660 (1998).

[5] S. Das Sarma, J. Fabian, X. Hu, and I. Žutić, Superlattices Microstruct. **27**, 289 (2000).

[6] J.M. Kikkawa and D.D. Awschalom, Nature (London) **397**, 139 (1999).

[7] S.A. Wolf, D.D. Awschalom, R.A. Buhrman, J.M. Daughton, S. von Molnár, M.L. Roukes, A.Y. Chtchelkanova, and D.M. Trege, Science **294**, 1488 (2001).

[8] M.J. Gilbert and J.P. Bird, Appl. Phys. Lett. **77**, 1050 (2000).

[9] D. Loss and D.P. DiVincenzo, Phys. Rev. A **57**, 120 (1998).

[10] A. Imamoglu, D.D. Awschalom, G. Burkard, D.P. DiVincenzo, D. Loss, M. Sherwin, and A. Small, Phys. Rev. Lett. **83**, 4204 (1999).

[11] D.S. Saraga and D. Loss, Phys. Rev. Lett. **90**, 166803 (2003).

[12] R. Fiederling, M. Keim, G. Reuscher, W. Ossau, G. Schmidt, A. Waag, and L.W. Molenkamp, Nature (London) **402**, 787 (1999); Y. Ohno, D.K. Young, B. Beschoten, F. Matsukura, H. Ohno, and D.D. Awschalom, *ibid.* **402**, 790 (1999); P.R. Hammar, B.R. Bennett, M.J. Yang, and M. Johnson, Phys. Rev. Lett. **83**, 203 (1999); C.-M. Hu, J. Nitta, A. Jensen, J.B. Hansen, and H. Takayanagi, Phys. Rev. B **63**, 125333 (2001).

[13] E.I. Rashba, Fiz. Tverd. Tela (Leningrad) **2**, 1224 (1960) [Sov. Phys. Solid State **2**, 1109 (1960)]; Y.A. Bychkov and E.I. Rashba, J. Phys. C **17**, 6039 (1984).

[14] M.V. Berry, Proc. R. Soc. London, Ser. A **392**, 45 (1984).

[15] *Geometric Phases in Physics*, edited by A. Shapere and F. Wilczek (World Scientific, Singapore, 1989).

[16] P.D. Ye, D. Weiss, R.R. Gerhardts, M. Seeger, K. von Klitzing, K. Eberl, and H. Nickel, Phys. Rev. Lett. **74**, 3013 (1995).

[17] P. D. Ye, S. Tarucha, and D. Weiss, in *Proceedings of the 24th International Conference on The Physics of Semiconductors* (North Scientific, Singapore, 1998).

[18] S.V. Dubonos, A.K. Geim, K.S. Novoselov, J.G.S. Lok, J.C. Maan, and M. Henini, Physica E (Amsterdam) **6**, 746 (2000).

[19] A. Nogaret, S.J. Bending, and M. Henini, Phys. Rev. Lett. **84**, 2231 (2000).

[20] A. Stern, Phys. Rev. Lett. **68**, 1022 (1992).

[21] D. Loss, H. Schoeller, and P. Goldbart, Phys. Rev. B **48**, 15 218 (1993).

[22] S.A. van Langen, H.P.A. Knops, J.C.J. Paasschens, and C.W.J. Beenakker, Phys. Rev. B **59**, 2102 (1999); D. Loss, H. Schoeller, and P. Goldbart, *ibid.* **59**, 13 328 (1999).

[23] M. Popp, D. Frustaglia, and K. Richter, Phys. Rev. B **68**, 041303(R) (2003).

[24] D. Frustaglia, M. Hentschel, and K. Richter, Phys. Rev. Lett. **87**, 256602 (2001).

[25] R. Landauer, IBM J. Res. Dev. **1**, 233 (1957); M. Büttiker, Y. Imry, R. Landauer, and S. Pinhas, Phys. Rev. B **31**, 6207 (1985); Y. Imry, in *Directions in Condensed Matter Physics*, edited by G. Grinstein and E. Mazenko (World Scientific, Singapore, 1986); for presentations in reviews see Refs. 26 and 29.

[26] S. Datta, *Electronic Transport in Mesoscopic Systems* (Cambridge University Press, Cambridge, 1997).

[27] D.S. Fisher and P.A. Lee, Phys. Rev. B **23**, 6851 (1981).

[28] A.D. Stone and A. Szafer, IBM J. Res. Dev. **32**, 384 (1988).

[29] D.K. Ferry and S.M. Goodnick, *Transport in Nanostructures* (Cambridge University Press, Cambridge, 1997).

[30] H.U. Baranger, D.P. DiVincenzo, R.A. Jalabert, and A.D. Stone, Phys. Rev. B **44**, 10 637 (1991).

[31] Exceptions are, e.g., the numerical study of Berry phase effects in adiabatic spin-dependent transport (Refs. 24 and 32) and Refs. 33 and 34 addressing spin-orbit effects in quantum transport.

[32] D. Frustaglia and K. Richter, Found. Phys. **31**, 399 (2001).

[33] B.K. Nikolić and J.K. Freericks, cond-mat/0111144 (unpublished).

[34] T.P. Pareek and P. Bruno, Phys. Rev. B **65**, 241305(R) (2002).

[35] In the presence of a magnetic field $\vec{B}=\vec{\nabla}\times\vec{A}_{\rm em}$ the Rashba interaction takes the form $\mathcal{H}_{\rm so}=\alpha_{\rm R}\{\vec{\sigma}\times[\vec{p}+(e/c)\vec{A}_{\rm em}]\}_z/\hbar$.

[36] D. Frustaglia, Ph.D.-Thesis, Technische Universität Dresden, 2001.

[37] This generalizes the representation used by F. Mireles and G. Kirczenow (Ref. 38) to account for inhomogeneous magnetic fields and arbitrary 2D geometries.

[38] F. Mireles and G. Kirczenow, Phys. Rev. B **64**, 024426 (2001).

[39] The choice $\vec{A}_{\rm em}=B_{\rm i}\Theta(x)\Theta(L-x)\{z[1+(\pi/L)y]\cos[(\pi/L)x]\hat{x}+y\sin[(\pi/L)x]\hat{z}\}$ generates the in-plane field at $z=0$ introduced in Fig. 2. The δ-function-type fields arising from differentiation of the Heaviside step functions Θ cancel due to the vanishing z component of $\vec{A}_{\rm em}$ at $x=0$ and $x=L$. We further note that $\vec{\nabla}\cdot\vec{A}_{\rm em}=0$ for $z=0$.

[40] B.J. van Wees, H. van Houten, C.W.J. Beenakker, J.G. Williamson, L.P. Kouwenhoven, D. van der Marel, and C.T. Foxon, Phys. Rev. Lett. **60**, 848 (1988); D.A. Wharam, T.J. Thornton, R. Newbury, M. Pepper, H. Ahmed, J.E.F. Frost, D.G. Hasko, D.C. Peacock, D.A. Ritchie, and G.A.C. Jones, J. Phys. C **21**, L209 (1988); L.I. Glazman, G.B. Lesovik, D.E. Khmel'nitskii, and R.I. Shekhter, Pis'ma Zh. Éksp. Teor. Fiz. **48**, 218 (1988) [JETP Lett. **48**, 238 (1988)].

[41] In the considered case of Fig. 2 the region where the direction of the field changes significatively coincides with the entire length L of the conductor.

[42] The nth mode propagates along the x direction with velocity $v_x(n)=(v_{\rm F}^2-v_n^2)^{1/2}$, where $v_{\rm F}$ is the Fermi velocity, $v_n=(\hbar/m^*)k_n$ is the velocity in y direction and $k_n=(\pi/w)n$ is the corresponding quantized wave number.

[43] D. Loss, P. Goldbart, and A.V. Balatsky, Phys. Rev. Lett. **65**, 1655 (1990).

[44] H. Kohno, G. Tatara, and T. Ono (unpublished).

[45] Such fields, induced by currents through ~100 nm narrow pillars, were realized in the context of Oerstedt switching (Ref. 46). With current densities of order 10^7 A/cm^2 one can achieve field strengths of a few hundred mT.

[46] J.A. Katine, F.J. Albert, R.A. Buhrman, E.B. Myers, and D.C. Ralph, Phys. Rev. Lett. **84**, 3149 (2000).

[47] M. Popp, D. Frustaglia, and K. Richter, Nanotechnology **14**, 347 (2003).

[48] While y-polarized incoming spin states (anti)aligned with the local magnetic field stay (anti)aligned along their orbital paths in the adiabatic limit, z-oriented (orthogonal) initial spin states precess within a plane perpendicular to the local field during transport.

[49] M. Popp, Diplomarbeit, Universität Regensburg, 2002.

[50] D. Frustaglia and K. Richter, cond-mat/0309228, Phys. Rev. B (to be published).